Heat Transfer Engineering, 31(8):646–657, 2010

ISSN: 0145-7632 print / 1521-0537 online
DOI: 10.1080/01457630903466613

Taylor & Francis
Taylor & Francis Group

Experimental Investigation of Friction Factor in the Transition Region for Water Flow in Minitubes and Microtubes

AFSHIN J. GHAJAR, CLEMENT C. TANG, and WENDELL L. COOK
School of Mechanical and Aerospace Engineering, Oklahoma State University, Stillwater, Oklahoma, USA

A systematic and careful experimental study of the friction factor in the transition region for single-phase water flow in mini- and microtubes has been performed for 12 stainless-steel tubes with diameters ranging from 2083 μm to 337 μm. The pressure drop measurements were carefully performed by paying particular attention to the sensitivity of the pressure-sensing diaphragms used in the pressure transducer. Experimental results indicated that the start and end of the transition region were influenced by the tube diameter. The friction factor profile was not significantly affected for the tube diameters between 2083 μm and 1372 μm. However, the influence of the tube diameter on the friction factor profile became noticeable as the diameter decreased from 1372 μm to 337 μm. The Reynolds number range for transition flow became narrower with decreasing tube diameter.

INTRODUCTION

Due to rapid advancement in fabrication techniques, the miniaturization of devices and components is ever increasing in many applications. Whether it is in the application of miniature heat exchangers, fuel cells, pumps, compressors, turbines, sensors, or artificial blood vessels, a sound understanding of fluid flow in micro-scale channels and tubes is required. Indeed, within this last decade, countless researchers have been investigating the phenomenon of fluid flow in mini-, micro-, and even nanochannels. One major area of research in the phenomenon of fluid flow in mini- and microchannels is the friction factor. However, amid all the investigations in mini- and microchannel flow, there seems to be a lack in the study of the flow in the transition region. One obvious question is the location of the transition region with respect to the hydraulic diameter of the channel and the roughness of the channel. To successfully understand friction factor and the location of the transition region, a systematic experimental investigation on various hydraulic diameters of mini- and microchannels is necessary. However, the science behind these advanced technologies seems to be controversial, especially fueled by the experimental results of the fluid flow and heat transfer at these small scales.

On one hand, researchers have found that the friction factors to be below the classical laminar region theory [1, 2]. Meanwhile, some have reported that friction factor correlations for conventional sized tubes to be applicable for mini- and microtubes [3–5]. However, many recent experiments on small-sized tubes and channels have observed higher friction factors than the correlations for conventional-sized tubes and channels [6–11], and the cause of this discrepancy was attributed to surface roughness. Literature also highlights the importance of diameter measurement and difficulties associated with quantifying the effect of roughness. These difficulties are primarily due to the large number of parameters used in describing various roughness geometries.

In this study, mini- and microtubes are chosen over other noncircular channels to negate the effect of aspect ratio, which

This is an extended version of paper ICNMM-62281: An Experimental Study of Friction Factor in the Transition Region for Single Phase Flow in Mini- and Micro-Tubes, presented at the ASME Sixth International Conference on Nanochannels, Microchannels, and Minichannels, Darmstadt, Germany, June 23–25, 2008.

This work was partially funded by the Sandia National Laboratories, Albuquerque, New Mexico. Sincere thanks are offered to Micro Motion for generously donating one of the Coriolis flow meters and providing a substantial discount on the other one. Thanks are also due to Martin Mabry for his assistance in procuring these meters. The assistance of Rahul Rao in the experimental part of this study is greatly appreciated.

Address correspondence to Professor Afshin J. Ghajar, School of Mechanical and Aerospace Engineering, Oklahoma State University, Stillwater, OK 74078, USA. E-mail: afshin.ghajar@okstate.edu

may serve to alter flow characteristics at these small scales. The major objectives of this study are to accurately measure the pressure drop in mini- and microtubes over a wide range of Reynolds numbers from laminar to the turbulent region and to explore the start and end of the transition region in these small sized tubes.

LITERATURE REVIEW

A brief investigation of literature ranging from early papers to those that are more current presents us with highly contradictory results. In fact, these contradictions may better be labeled as widespread disparity. The early researchers observed lower friction factors while the later ones observed higher friction factors than predicted by theory. Despite this, it should be noted that the majority of the more recent researchers tend to observe results that agree with theory within calculated uncertainties. In spite of all the contradicting results available, the role that roughness, instrumentation, measurements, and dependence of diameter bring about in altering the flow characteristics at these micro-scales has been more or less acknowledged. Despite this acknowledgment, it is still not clear exactly what role these parameters play in influencing the flow characteristics.

Choi et al. [1] performed pressure drop measurements on fused-silica microtubes with dry nitrogen gas as the test fluid. The diameters ranged from 3 to 81 μm and the roughness measurements confirmed that the microtubes were essentially smooth. They found the f·Re value to be around 53, which was considerably less than the theoretical value of 64. Similar results were obtained for the turbulent flow data. The authors also observed that the measurements were not influenced by the roughness of the microtubes.

Similar results were obtained by Yu et al. [2] in their experiment using water and nitrogen gas. The microtubes used were from the same manufacturer (Polymicro Technologies) as for Choi et al. [1]. They found the f·Re product to be 50.13, which is considerably lower than the classical value of 64. Both Choi et al. [1] and Yu et al. [2] used compressible flow analysis for the nitrogen test fluid. Friction factor was calculated using the Fanno-line expression in both cases.

Hwang and Kim [3] investigated the pressure drop characteristics of R-134a in stainless-steel tubes with diameters of 244, 430, and 792 μm. They found that within experimental uncertainty, conventional theories are able to predict the experimental friction factors. The authors found no evidence of early transition and they reported the onset of transition Reynolds number occurred slightly below 2,000.

Yang and Lin [4] investigated water flow through stainless-steel tubes with diameters ranging from 123 to 962 μm. They found that the friction factor results correlate well with correlations for conventional tubes. There was no significant effect of size on their results within the diameter range of their reported work. Transition range was observed from Reynolds number of 2,300 to 3,000.

Rands et al. [5] measured the frictional pressure drop and temperature induced by viscous heating for water flowing through fused-silica microtubes with diameters from 32.2 to 16.6 μm. The results from their work were confirmed with classical laminar flow behavior at low Reynolds number. The onset of transition region was observed at the Reynolds numbers of 2,100 to 2,500.

Mala and Li [6] analyzed water flowing through fused-silica and stainless-steel tubes ranging from 50 to 254 μm. Contrary to the previous researchers, they found friction factor values larger than what the theory predicted. Moreover, they also observed a dependence of the f·Re product on Reynolds number. Early transition in Reynolds number range of 300 to 900 was reported, and surface roughness was proposed as a significant cause of that early flow transition.

Celata et al. [7] performed pressure drop tests using R-114 in a 130 μm microtube. The Reynolds numbers investigated ranged from 100 to 8,000. Transition was observed to be in the Reynolds number range of 1,880 to 2,480. In the laminar region, the experimental values matched well with the theoretical predictions until the Reynolds number of 585. For Reynolds numbers greater than 585, higher friction factor values were observed. The authors attributed this deviation from theory to roughness of the stainless-steel microtube.

Kandlikar et al. [8] investigated the effect of roughness on pressure drop in microtubes. The roughness was changed by etching the tubes with different acids. They observed that for larger tubes (1067 μm), the effect of roughness is negligible. For smaller tubes (620 μm), increases in roughness resulted in higher pressure drop accompanied by early transition.

Li et al. [9] investigated flow through glass microtubes (79 to 449 μm in diameter), silicon microtubes (100 to 205 μm in diameter), and stainless-steel microtubes (129 to 180 μm in diameter). They found that the f·Re in laminar region for smooth tubes was nearly 64, while the results for rough tubes with peak–valley roughness of 3 to 4% showed 15 to 37% higher than the classical f·Re value of 64. Based on flow characteristics, Li et al. [9] concluded that the onset of transition region occurred at the Reynolds numbers of 1,700 to 2,000.

Zhao and Liu [10] conducted pressure drop studies on smooth quartz-glass tubes and rough stainless-steel tubes of varying diameters. They observed that in the laminar regime, experimental results agreed well with theoretical values. However, early transition at Reynolds numbers ranging from 1,100 to 1,500 (for smooth microtubes) was recorded. For rough microtubes (with $\varepsilon/D = 0.08$), laminar theory agrees only until the Reynolds number of 800, where similar early transition was observed.

Tang et al. [11] investigated the flow characteristics of nitrogen and helium in stainless-steel and fused-silica tubes of various diameters. They observed that the friction factors in stainless-steel tubes are much higher than the theoretical correlation for the laminar region, deviating by as much as 70% for a tube diameter of 172 μm. Friction factors for the smoother walled fused-silica tubes were found to be in relative agreement with the theory for conventional-sized tubes. The positive

deviation was attributed to the roughness and was found to increase with decreasing diameter, bringing up questions of both diameter and roughness effects. They also acknowledged the fact that accurate measurement of the inner diameter is essential, citing it as a possible factor in leading to higher friction factors.

In a review by Kandlikar [12], he suggested that the uncertainties in the experiments by Nikuradse [13] in the laminar region were very high, and the conclusion regarding the absence of roughness effects in the laminar region is questionable. Noticing that mini- and micro-fluidic systems routinely violate the 5% relative roughness threshold set by Moody, Colebrook, and Nikuradse, Kandlikar et al. [14] and Taylor et al. [15] proposed modifying the Moody diagram to reflect new experimental data. Kandlikar et al. [14] proposed a new effective flow diameter based on the effect of flow constriction due to roughness elements,

$$D_{cf} = D - 2\varepsilon \tag{1}$$

where D_{cf} is the constricted flow diameter, D is the tube inner diameter, and ε is the roughness height. One may consider that the constricted flow diameter (D_{cf}) corresponds to the free flow area. This concept proposed by Kandlikar et al. [14] is very much like the effect of *vena contracta* seen in orifice meters, where a contraction coefficient is used to relate the orifice area to the *vena contracta* area. The relation of the friction factor (f) with the friction factor based on the constricted flow diameter (f_{cf}) is

$$f_{cf} = f\left(\frac{D_{cf}}{D}\right)^5 \tag{2}$$

Based on the constricted flow diameter, the Reynolds number is then expressed as

$$Re_{cf} = \frac{4\dot{m}}{\pi D_{cf}\mu} \tag{3}$$

Brackbill and Kandlikar [16] experimentally investigated the effect of relative roughness on friction factor and critical Reynolds number for mini- and microchannels. In their experiments, the Reynolds numbers were varied from 30 to 7,000 for hydraulic diameters ranging from 1,084 to 198 μm with relative roughness ranging from 0 to 5.18%. To obtain uniform roughness on the channel surface, a systematic approach was taken by sanding the surface 45 degrees in both directions from the axis along the channel length [16]. An in-depth discussion in the parameterization of relative roughness for different machined surfaces using this surface roughening method is documented by Young et al. [17]. Contrary to the findings of Nikuradse [13], Brackbill and Kandlikar [16] observed that there was indeed the effect of roughness in the laminar region. Figure 1a illustrates the friction factor versus Reynolds number plot by Brackbill and Kandlikar [16] for channels with varying relative roughness. Clearly, as shown in Figure 1a, roughness effects played a role in the laminar region, and the effects increased with higher

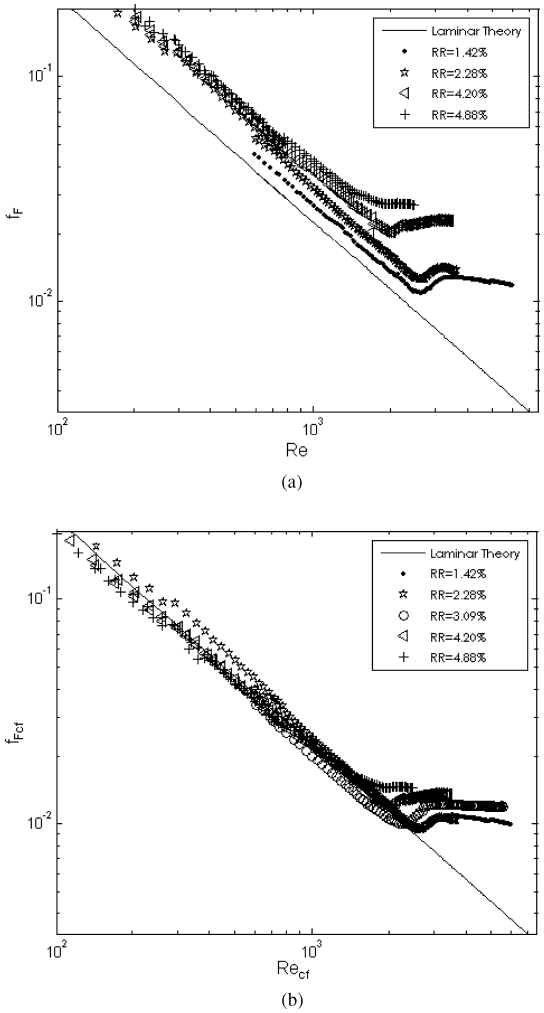

Figure 1 Friction factor versus Reynolds number plotted by Brackbill and Kandlikar [16] for channels with various relative roughness: (a) without using constricted flow parameters, (b) with using constricted flow parameters.

relative roughness. By including the constricted flow hydraulic diameter ($D_{h,cf}$) to the experimental data, Brackbill and Kandlikar [16] observed that the agreement between the experimental data and laminar flow theory for friction factor was significantly improved (Figure 1b). In addition, they also observed a trend relating the critical Reynolds number and the relative roughness. To predict the onset of transition region, Brackbill and Kandlikar [16] recommended a correlation for the critical Reynolds number and the relative roughness based on the constricted flow hydraulic diameter,

$$Re_{c,cf} = Re_{c,o} - \frac{Re_{c,o} - 800}{0.08}\left(\frac{\varepsilon}{D_{h,cf}}\right) \quad \text{for}$$

$$0 \le \varepsilon/D_{h,cf} \le 0.08 \tag{4}$$

$$Re_{c,cf} = 800 - 3270(\varepsilon/D_{h,cf} - 0.08) \quad \text{for}$$

$$0.08 \le \varepsilon/D_{h,cf} \le 0.15$$

where the critical Reynolds number for smooth channels ($Re_{c,o} = 2{,}500$) was used [16]. Equation (4) was developed for channels and has only been verified with data for mini- and microchannels from [16] and [18]. The correlation has an average absolute error of 13% [16].

Recently, Celata et al. [19] conducted experimental studies for compressible flow of nitrogen gas inside microtubes ranging from 30 to 500 μm with relative roughness of 1% or less. The results they found indicated that the agreement of friction factor in laminar flow with theory for conventional sized tubes is excellent. For microtubes with diameter of 100 μm or less, Celata et al. [19] reported that when $Re > 1{,}300$ the friction factor tends to deviate from the Poiseuille law and attributed the deviation to acceleration associated with compressibility effect. Furthermore, their studies observed no evidence of early transition, with respect to conventional-size pipes, with the critical Reynolds number for transition ranging from 2,160 to 4,430, and critical Reynolds number showed no dependence on tube length to diameter ratio.

In most mini- and micro-fluidic systems, the flow regions are likely to be mainly laminar and transitional. The other question that needs to be addressed is the location (start and end) of the transition region and its shape for different diameters. Literature has reported the onset of transition to be either early [6, 8, 10, 16] or in agreement with conventional-sized tubes and channels [4, 5]. The discrepancies in whether size and roughness effects contribute to the increase of friction factors, and lower critical Reynolds numbers (early transition) may be attributed to inadequacies in instrumentation. While accurate measurement of inner diameter is certainly acknowledged to be of great importance, it is shown in this article that the sensitivity of the instrument providing pressure drop measurements should be of equal if not greater concern. This is discussed in detail in the Results and Discussion section of this article.

EXPERIMENTAL SETUP

Experimental Apparatus

The experimentation for this study was performed using a relatively simple but highly effective apparatus. The apparatus used was designed with the intention of conducting highly accurate pressure drop measurements. In addition to accurate measurements, the apparatus was also designed to be versatile, accommodating the use of multiple diameters and lengths of test sections. The apparatus consists of four major components. These are the fluid delivery system, the flow meter array, the test section assembly, and the data acquisition system. Each of these different components is discussed independently. An overall schematic for the experimental test apparatus is shown in Figure 2.

The fluid delivery system is a pneumatic and hydraulic combination, consisting of a high-pressure cylinder filled with ultra-high-purity nitrogen in combination with a stainless-steel pressure vessel. The system is an open loop. Thus, after the working fluid passes through the apparatus, it is passed into a sealed collection container and recycled manually. Nitrogen in the high-pressure cylinder is pressurized to 17.2 MPa by the distributor. This pressurized nitrogen is then fed to the stainless-steel pressure vessel via a two-phase regulator and line. The working fluid, distilled water for the purposes of this research, is stored in the stainless-steel pressure vessel. As the pressurized nitrogen is fed into the stainless-steel pressure vessel, the working fluid is forced up a stem extending to the bottom of the vessel, out of the pressure vessel, and through the flow-meter array and test section. An Airgas regulator is used for the purposes of controlling the pressure of the nitrogen inlet to the stainless-steel pressure vessel. This dual-stage regulator is capable of providing pressures ranging from 0 to 1.72 MPa. The stainless-steel pressure vessel used is an Alloy Products model 72–05, providing a maximum working pressure of 1.37 MPa and a capacity of 19.0 L.

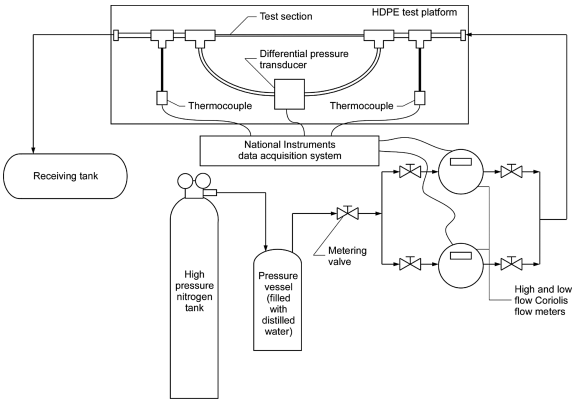

Figure 2 Schematic of the experimental setup.

After exiting the pressure vessel, the distilled water travels to the flow-meter array. The flow rate of the water entering the array is further regulated using a Parker N-Series model 6A-NLL-NE-SS-V metering valve, which allows fine-tuning of the flow rate. Fluid passes through the metering valve and into one of the two Micro Motion Coriolis flow meters. Two flow meters are necessary in order to accommodate the large range of flow rates that are studied using the experimental apparatus. The larger of the two meters used is a CMF025 coupled with a model 1700 transmitter. This meter is designed to measure mass flows ranging from 54 to 2,180 kg/h for liquids. Within this range of mass flows, this meter is accurate to 0.05%. However, much smaller flow rates can be measured with very little loss in accuracy. The smaller of the two meters is a Micro Motion model LMF3M, coupled with an LFT transmitter. This second meter is designed to measure mass flows ranging from 0.001 to 1.5 kg/h.

After passing through the flow-meter array, fluid enters the test section assembly via a second section of PFA tubing to the test section assembly. The test section assembly contains the test section as well as the equipment necessary for measurement of

inlet and outlet fluid temperatures and pressure drop. This test section was constructed for the incorporation of a very broad range of test section diameters, encompassing both mini and micro tube sizes. In experimentation to date, research has been conducted on 12 different tube sizes. The inner diameters of these tubes vary from 2,083 to 337 μm. All of the tubes used are available from Small Parts, Inc. The tubes used are stainless-steel type 304 hypodermic tubes with factory-cut lengths of 30.5 cm (for $2083 \leq D \leq 667$ μm) and 15.2 cm (for $559 \leq D \leq 337$ μm). Since the friction factor measurements are conducted for fully developed flow, the length of the tube bears no effect on the results. As pointed out by Krishnamoorthy and Ghajar [20], the effect of tube length on the friction factor is negligible as long as the flow is fully developed.

The pressure transducer used for pressure drop measurements is a Validyne model DP15. This pressure transducer utilizes a series of interchangeable diaphragms to provide the ability to measure a very large range of differential pressures. The research facilities used for experimentation have different pressure transducer diaphragms to encompass a range of differential pressures from 1.38 to 1,380 kPa. The Validyne pressure transducer has an accuracy of ±0.25% full scale of the diaphragm used. Careful attention is given to ensure that the range of the diaphragm used is conducive to the pressure being measured. The use of the numerous interchangeable diaphragms is an important factor in ensuring the accuracy of the pressure drop measurements.

All data from the thermocouples and pressure transducer are acquired using a National Instruments data acquisition system and recorded with the laboratory PC (personal computer) and LabView software.

Calibration of Instruments

Nine different pressure transducer diaphragms are used to cover differential pressures ranging from 1.38 to 1,380 kPa. Calibrations are performed at the beginning of each experiment with the appropriate diaphragms. During calibration, the voltage output of the differential pressure transducer at numerous applied pressures is compared against the reading of one of the four research grade test gauges. Of these four gauges, the highest rated in terms of pressure is a Perma-Cal 2070 kPa test gauge with an accuracy of ±0.25% full scale. For lower pressures, two Wika test gauges, also with accuracy of ±0.25% full scale, are used. The first of these has a pressure rating of 1,100 kPa and the second is rated up to 103 kPa. For low-pressure diaphragm calibration a Cole-Palmer digital manometer is used. This instrument has a pressure rating of 103 kPa, an accuracy of ±0.3% full scale, and a resolution of 69 Pa.

The Micro Motion Coriolis flow meters are factory calibrated as well. For the CMF-025, the manufacturer's specified tolerance for calibration error is ±0.1%. For the LMF3M, the manufacturer's specified calibration tolerance is ±1.0%. For both of these meters, in-laboratory calibration consisted of checking the manufacturer's calibrations over a range of flow rates via timed collection of fluid passing through the meters. In addition, the maximum and minimum milliamp outputs of the CMF-025 were tuned to improve the resolution of the meter.

Experimental Uncertainty

Developing an understanding of the experimental uncertainty in the calculated friction factor is absolutely necessary. From the measured pressure drop data, the friction factor can be calculated with

$$f = \frac{2\Delta p D}{\rho L V^2} = \frac{\Delta p D^5 \pi^2 \rho}{8 L \dot{m}^2} \tag{5}$$

The uncertainty in the pressure drop measurement can be readily obtained from the manufacturer's specifications on the Validyne pressure transducer. As has been previously stated, this specification is given as ±0.25% of the full-scale reading of each diaphragm used. Diaphragms were carefully selected during experimentation in order to obtain the highest accuracies possible. The worst-case scenario occurs with small tube size and low Reynolds number. In this region, the uncertainty in the pressure drop measurement can be estimated at ±1.0%. It is more representative to look at intermediately sized tubes and/or flow rates through the transition and turbulent regions. Uncertainty of the pressure drop measurement in these areas drops to ±0.4%.

The uncertainty in mass flow rate measurement given by the Micro Motion flow meter specifications for the CMF-025 meter is ±0.05%. For the LMF3M meter, an uncertainty of reading of ±0.50% is given. However, it has to be taken into consideration that the larger meter is being utilized at flow rates lower than its range in order to cover the entire range of flow rates for all of the tubes under research. Based upon uncertainty equations given in the Micro Motion specifications, the worst-case scenario accuracy between the two flow meters is ±1.8%. Both the use of the LMF3M and the under-ranging of the CMF-025 occur at smaller tube sizes and lower Reynolds numbers. Thus, it is necessary to calculate uncertainty for either of the meters running within their specified mass flow ranges and to estimate uncertainty when the CMF-025 is pushed to its lowest range of measurement.

Uncertainty in tube length is determined by the accuracy of the cutting of the high-density polyethylene tube cradles. The cradles serve as a reference point for the mounting of the different tube sections in order to ensure consistency. Measured uncertainty in the cradle lengths is ±0.26% of length.

Due to the fact that uncertainty in both the Validyne pressure transducer and the Micro Motion meters is dependent upon tube size and Reynolds number, three different uncertainty values have been established. In order to quantify the overall uncertainty, analysis was conducted using the method described by Kline and McClintock [21]. In the case of larger tube sizes and higher Reynolds numbers, the CMF-025 meter is used and is

functioning at the manufacturer's specified uncertainty level. The pressure transducer is operating at the better of its two calculated uncertainty levels. Taking this into consideration, the overall uncertainty is calculated at ±0.83%. As the tube size and Reynolds number decrease, the CMF-025 meter begins to operate under range. In this area, the pressure transducer is considered to be operating at the lesser of its two uncertainty levels. In this range, the overall uncertainty associated with the experimental apparatus is calculated to be ±2.78%. Finally, at the lowest ranges of tube size and Reynolds number, the LMF3M meter is used. In this area, the pressure transducer is still operating at the lesser of its two uncertainty levels. For this lowest Reynolds number and smallest tube size situation, the overall uncertainty decreases to ±1.51%. The uncertainties discussed in this section are for the experimental results when the pressure-sensing diaphragms were used appropriately for the measured pressure drop ranges.

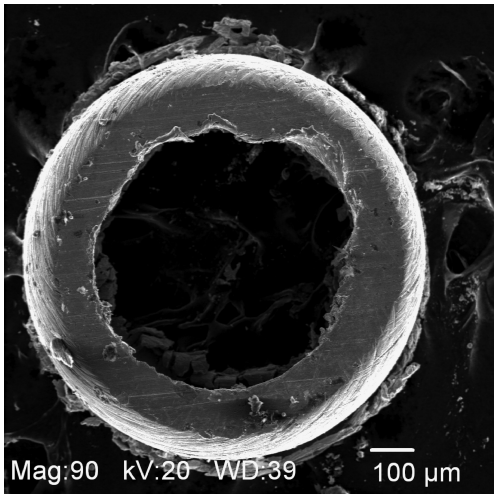

Figure 3 SEM image of a 584 ± 38 μm (manufacturer's specification) diameter stainless-steel tube; based on this SEM image, the tube diameter was found to be 574 μm.

Diameter and Surface Roughness Verification

Since the mini- and microtubes under research were purchased from an outside source, data obtained from these tubes are only as accurate as the manufacturer's specifications. The diameters of the tubes as well as the roughness of the inner walls of the tubes are of particular concern due to the type of research being undertaken. In order to ensure that the data recorded were of the highest quality possible, it was deemed necessary to determine the degree of accuracy of the manufacturer's specifications. In order to do this, both the scanning electron microscope (SEM) and the scanning probe microscope (SPM) at the Oklahoma State University Microscopy Laboratory were utilized. Diameter measurements were taken using the SEM, while roughness measurements were taken using the SPM.

Two different tube sizes were examined using the SEM in order to check the accuracy of the manufacturer's tolerances. The first of these two tubes had an inner diameter and tolerance of 5330 ± 76 μm. The second tube examined had an inner diameter and tolerance of 584 ± 38 μm. Thus, a broad range of tube size was covered between the two tubes examined. Imaging was done using the JEOL JXM 6400 scanning electron microscope system in combination with a digital camera system. The resolution of the microscope ranged from 30 to 50 nm. Once images had been captured, it was possible to determine image pixel size in terms of length scale. With a known pixel-to-length scale, the inner diameter of the tubes could be estimated from the SEM images.

For the first tube with the manufacturer-specified inner diameter of 5330 ± 76 μm, the average inner diameter was estimated to be 5,280 μm from the SEM image. For the second tube with the manufacturer-specified inner diameter of 584 ± 38 μm, the average inner diameter was estimated to be 574 μm from the SEM image (see Figure 3). The SEM imaging of these two tubes verified that the manufacturer's specifications of the tube diameters and tolerances are verifiable and reasonably dependable.

Roughness measurements were conducted using a SPM station in combination with Digital Instruments Multimode V electronics and an optical microscope for tip positioning. The system used is capable of three-dimensional (3-D) spatial mapping and an ultimate resolution of 0.1 nm laterally and 0.01 nm vertically. Scans were taken of multiple sections of two stainless-steel tubes with different inner diameters: 5,330 μm and 2,390 μm. Roughness data were taken from three different sections of each of these tubes. In order to negate the effect of the curvature of the tubes upon the roughness measurement generated by the SPM, a flattening feature was utilized. From the SPM, information such as average roughness (R_a), maximum roughness profile peak height (R_{max}), and root mean square roughness (R_q) of the samples was obtained. The topographic image for a section of the 5,330 μm diameter tube is shown in Figure 4.

From the SPM measurements, the inner surface of the 5,330 μm diameter stainless-steel tube has average roughness (R_a), maximum roughness profile peak height (R_{max}), and root mean square roughness (R_q) of 240 nm, 2,628 nm, and 292 nm, respectively. In similar manner, the inner surface of the 2,390 μm diameter stainless-steel tube has R_a, R_{max}, and R_q of 150 nm, 1,710 nm, and 194 nm, respectively. Some variability was found between the two tubes, though this was to be expected. The manufacturer specified an inner wall root mean square roughness of 410 nm. Thus, the root mean square roughness measured by the SPM for each of the two tubes was within the manufacturer's specifications.

When compared with the roughness results documented by Young et al. [17], the maximum roughness profile peak height (R_{max}) for both stainless-steel tubes falls between the maximum roughness profile peak height of milled stainless-steel surface ($R_{max} = 3210$ nm) and ground stainless-steel surface ($R_{max} = 999$ nm). It should be noted that measurements by Young et al. [17] were from surface roughness that was created systematically to be uniform and aligned. On the other hand, the tubes

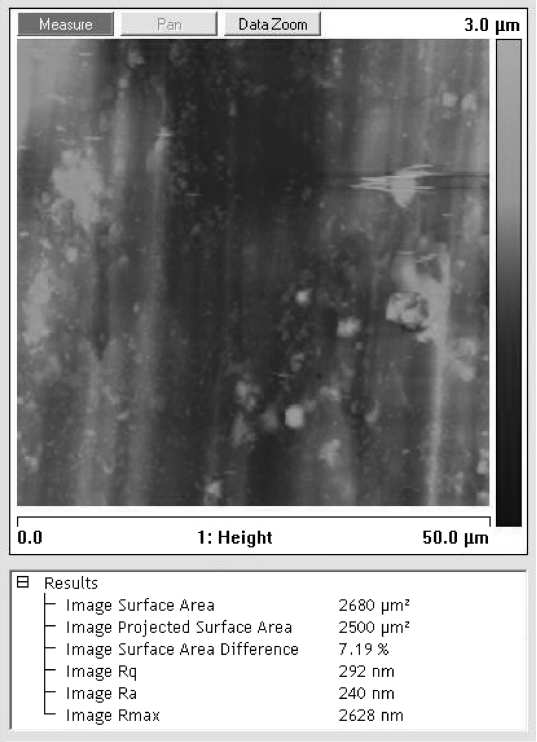

Figure 4 SPM topographic image for a section of a 5,330 µm inner diameter stainless-steel tube ($R_a = 240$ nm, $R_{max} = 2{,}628$ nm, $R_q = 292$ nm).

used in this study were obtained commercially, and thus the uniformity and alignment of the surface roughness in these tubes are uncertain.

Based on the inner diameter tolerances specified by the manufacturer and the results from both SPM and SEM measurements, the constricted flow diameter (D_{cf}), proposed by Kandlikar et al. [14] can be determined. Having known the constricted flow diameter (D_{cf}), the roughness height (ε) of the tubes can be estimated using the concept of constricted flow diameter—see Eq. (1)—proposed by Kandlikar et al. [14]. As shown in Figure 3, the irregularities in the tube and the tolerances of the inner diameter can result in much larger roughness height (ε) than the average roughness (R_a) measured by the SPM.

RESULTS AND DISCUSSION

The review documented by Krishnamoorthy and Ghajar [20] pointed out the need for further experiments to confirm the start and end of transition region in mini- and microtubes. In large part, this need for further experimentation is exemplified by the highly contradictory observations that have been reported by various investigators. The disparity found in the literature may be attributed to factors such as tube diameter, surface roughness, experimental facilities, and instrumentation. Without any doubt, the sensitivity of the instruments used in the measurement of pressure drop plays one of the most crucial roles in collecting accurate data. In addition, in properly addressing the effect of tube diameter on pressure drop for flow in mini- and microtubes, the importance of systematically investigating various tube sizes cannot be overlooked.

In order to be able to clearly pick up the transition region along with the laminar and turbulent regions, the sensitivity of the pressure-sensing diaphragms used in the Validyne DP15 pressure transducer had to be given meticulous consideration. Even the numerous studies that covered the laminar and turbulent regions fail to explicitly capture the transition region. In many cases, this failure may be attributed to the questionable sensitivity of the instrumentation used. The dilemma that arises from this is that if one is not confident with the results for the transition region, then the confidence in the results for laminar and turbulent regions is also questionable.

To properly recognize sensitivity for each pressure-sensing diaphragm, it is necessary to collect pressure drop data for the entire pressure-sensing range of each diaphragm before changing to the next diaphragm. Collecting pressure drop data through the entire pressure-sensing range of each diaphragm further enhances collection of accurate data. The overall uncertainty associated to each pressure-sensing diaphragm was estimated to be roughly $\pm 1.5\%$ full scale of the diaphragm's pressure-sensing range. This $\pm 1.5\%$ uncertainty includes the uncertainties of the pressure transducer, the pressure gages used for calibrating the pressure diaphragms, and the standard deviation of the pressure drop data. An uncertainty of $\pm 1.5\%$ full scale of the diaphragm's pressure-sensing range implies that a 345-kPa pressure diaphragm would have an uncertainty of ± 5.18 kPa.

Figure 5 illustrates the comparison of the friction factor data points measured using various pressure-sensing diaphragms for 1,600 and 1,067 µm diameter stainless-steel tubes. Figure 5a brings out the obvious scenario that using both 55.2 and 138 kPa pressure diaphragms for $700 < Re < 3{,}500$ would easily bring one to conclude that the higher friction factor values are due to surface roughness. The appropriate error bars, based on the uncertainty of $\pm 1.5\%$ full scale of the diaphragm's pressure-sensing range, are attached on two selected data points obtained by 55.2 and 138 kPa pressure diaphragms to illustrate their uncertainties. The data point measured by the 55.2 kPa pressure diaphragm at $Re = 1{,}100$ carried an uncertainty of $\pm 28\%$, while the data point measured by the 138 kPa pressure diaphragm at $Re = 1{,}400$ carried an uncertainty of $\pm 46\%$. In addition, the data point measured by the 138 kPa pressure diaphragm at $Re = 1{,}400$ shows the error bar with a 14% extension below the $f = 64/Re$ line. Such scenario implies the possibility of having a wrong conclusion that the value of $f \cdot Re$ is 55 rather than the conventional value of 64. For comparison purposes, in Figure 5a error bars are also attached on two selected data points obtained by the 3.45 and 13.8 kPa pressure diaphragms, which show significantly lower uncertainties than the error bars on the data points obtained by the 55.2 and 138 kPa pressure diaphragms. As shown in Figure 5a, pressure diaphragms with ratings of 13.8 kPa or lower would be appropriate for $Re < 3{,}500$, and pressure diaphragms with ratings of 55.2 kPa or higher would be appropriate for $Re > 3{,}500$. For $500 < Re < 1{,}700$, data points

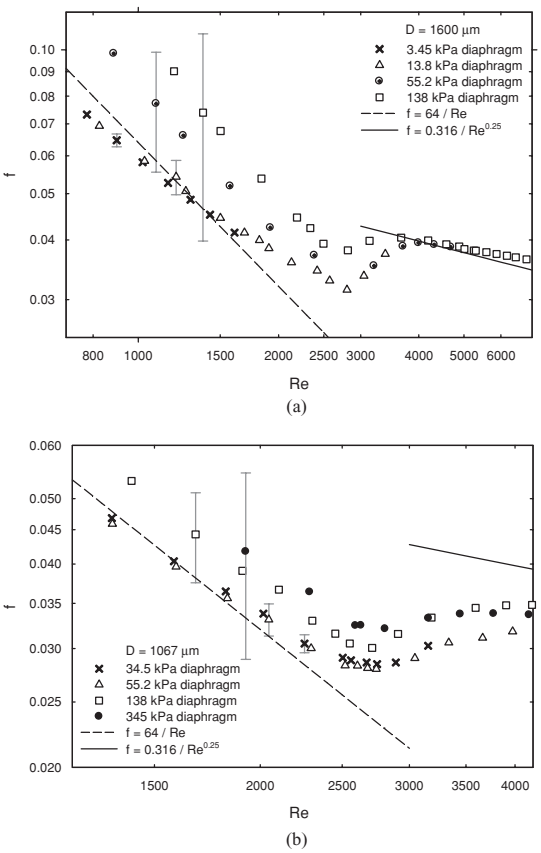

Figure 5 Comparison of results measured by various pressure-sensing diaphragms for two different tubes: (a) 1,600 μm diameter tube, (b) 1,067 μm diameter tube.

measured by the 13.8 kPa pressure diaphragm were also verified by the 3.45 kPa pressure diaphragm to be within experimental uncertainties. Similarly, data points measured by the 55.2 kPa pressure diaphragm were also verified by the 138 kPa pressure diaphragm to be within experimental uncertainties for $3500 < \mathrm{Re} < 5{,}500$.

Figure 5(b) illustrates that the proper selection of pressure-sensing diaphragms is essential to accurately measure friction factor in the transition region. The appropriate error bars, based on the uncertainty of $\pm 1.5\%$ full scale of the diaphragm's pressure-sensing range, are attached on a data point measured by a 138 kPa pressure diaphragm at $\mathrm{Re} = 1{,}700$, and another data point measured by a 345 kPa pressure diaphragm at $\mathrm{Re} = 1{,}900$ (Figure 5b). The data point measured by the 138 kPa pressure diaphragm at $\mathrm{Re} = 1{,}700$ carried an uncertainty of $\pm 15\%$, while the data point measured by the 345 kPa pressure diaphragm at $\mathrm{Re} = 1{,}900$ carried an uncertainty of $\pm 31\%$. In addition, the data point measured by the 345 kPa pressure diaphragm at $\mathrm{Re} = 1{,}900$ shows the error bar with a 14% extension below the $f = 64/\mathrm{Re}$ line. As seen previously in Figure 5a, this scenario shown in Figure 5b also implies the possibility of having a wrong conclusion that the value of $f \cdot \mathrm{Re}$ is 55 rather than the conventional value of 64. For comparison purposes, in Figure 5b error bars are also attached on two selected data points obtained by the 34.5 and 55.2 kPa pressure diaphragms which show significantly lower uncertainties than the error bars on the data points obtained by the 138 and 345 kPa pressure diaphragms. The discrepancies between the data points measured by the 138 kPa and 345 kPa pressure diaphragms show that these diaphragms could not accurately capture the transition region. The actual friction factor values were accurately measured by the 55.2 kPa diaphragm and verified by the 34.5 kPa diaphragm to be within experimental uncertainties. At the trough of the transition region ($\mathrm{Re} \approx 2{,}750$), the data measured by the 345 kPa diaphragm was 15% higher than the data measured by the 55.2 kPa diaphragm. The data measured by the 138 kPa diaphragm at $\mathrm{Re} \approx 2{,}750$ was 8% higher than the data measured by the 55.2 kPa diaphragm.

Based on the illustrations of Figure 5, improper use of pressure-sensing diaphragm could easily lead to erroneous conclusions about the flow phenomena in the microtubes tested. It should be noted that the ability to capture transition decays quite rapidly when diaphragms inappropriate to the range of pressure drop under investigation are utilized. Thus, extreme care in diaphragm selection is imperative in order to capture the transition region with the greatest possible accuracy. Even small failures in terms of accuracy can lead to flatter transition regions, leaving the actual physics of the flow unobserved. With the effect of surface roughness and diameter in microtubes still largely unexplored, these types of failures are unacceptable. Although it seems trivial to discuss the sensitivity of the pressure diaphragm, Figures 5a and b clearly illustrate the consequences of ignoring it. It should be noted that all the friction factor data reported in Figures 6 to 9 have an uncertainty of $\pm 1.5\%$.

The experimental results of 12 different stainless-steel tubes with diameters ranging from 2,083 to 337 μm were investigated in detail with regard to the laminar, transition, and turbulent regions over Reynolds numbers ranging from 500 to 10,000. The experimentally determined friction factor in the laminar region was compared with the conventional friction factor equation for fully developed laminar flow, $f = 64/\mathrm{Re}$. For turbulent region, the experimental friction factor was compared with the Blasius friction factor equation for turbulent flow, $f = 0.316/\mathrm{Re}^{0.25}$. A representative of the experimental results for the friction factor

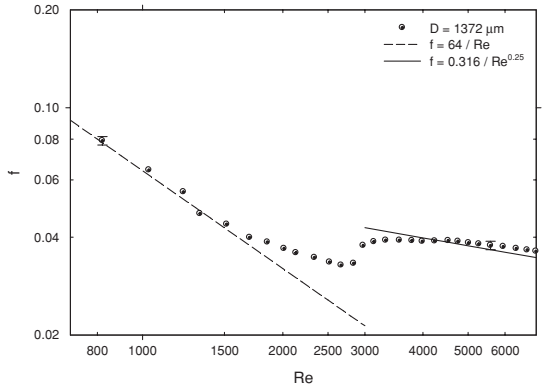

Figure 6 Experimental friction factor of 1372 μm diameter stainless-steel tube.

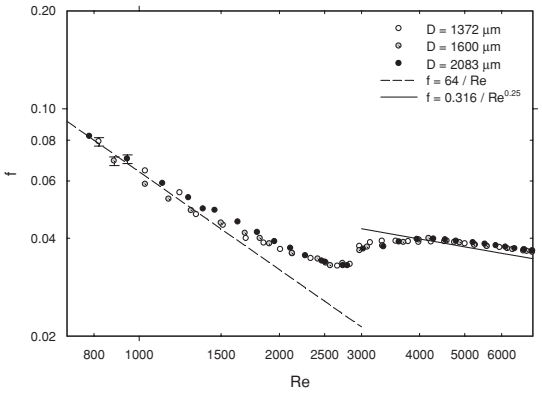

Figure 7 Transition region of stainless-steel tubes with diameters from 2,083 to 1,372 μm.

of the 1,372 μm diameter stainless-steel tube is shown in Figure 6. As illustrated in Figure 6, the onset of transition for the 1372 μm diameter tube is at Reynolds number of 1,900, and the end of transition is at Reynolds number of 4,000.

Based on the experimental friction factors, the transition region can be estimated by locating the Reynolds numbers where the friction factor departs from the laminar line and merges with the turbulent line. The transition Reynolds number ranges summarized in Table 1 were determined by using a 5% deviation criterion from the laminar and turbulent lines. According to our experimental uncertainty analysis, the maximum error in friction factor measurements was estimated to be no more than 3%, and the 5% deviation criterion was used to encompass the experimental uncertainty. In the estimation of the transition Reynolds number range for each tube diameter, the transition region begins with the first data point that is 5% higher than the laminar line, and ends with the data point that is 5% lower than the perceived turbulent line. The perceived turbulent line is a straight line connecting the data points in the turbulent region (Re $>$ 4,000) on the base-10 logarithms friction factor versus Reynolds number plot.

The experimental friction factor results provided an interesting observation. The decrease in tube diameter from 2,083 to 667 μm actually delayed the onset of transition region. For

Table 1 Summary of transition Reynolds number ranges for various stainless-steel tube sizes

Tube ID (μm)	Transition range	Tube ID (μm)	Transition Range
2083	1,500 $<$ Re $<$ 4,000	732	2,200 $<$ Re $<$ 3,000
1600	1,700 $<$ Re $<$ 4,000	667	2,200 $<$ Re $<$ 3,000
1372	1,900 $<$ Re $<$ 4,000	559	1,900 $<$ Re $<$ 2,500
1067	2,000 $<$ Re $<$ 4,000	508	1,700 $<$ Re $<$ 2,100
991	2,000 $<$ Re $<$ 4,000	413	1,500 $<$ Re $<$ 1,900
838	2,200 $<$ Re $<$ 4,000	337	1,300 $<$ Re $<$ 1,700

the 2,083 μm diameter tube, the transition region began at a Reynolds number of 1,500. As the tube diameter decreased to 667 μm, the Reynolds number for the onset of transition region was shifted to approximately 2,200 (see Table 1). The end of the transition region for tubes with diameters from 2,083 to 838 μm is consistently located at a Reynolds number of 4,000. However, for tube sizes of 732 and 667 μm, the end of the transition region shifted forward to a Reynolds number of 3,000. Further decrease in the tube diameter from 667 to 337 μm caused the onset of the transition region to shift from a Reynolds number of 2,200 to 1,300, while the end of the transition region shifted from a Reynolds number of 3,000 to 1,700. The experimental results indicated that the Reynolds number range for transition flow becomes narrower with the decrease in tube diameter.

By focusing on the transition region, the effect of tube diameter on the friction factor profile can be clearly seen. The friction factor profiles of the 12 stainless-steel tubes in the transition region are shown in Figures 7 to 9. Figure 7 shows that the decrease in tube diameter from 2,083 to 1,372 μm did not significantly affect the profile of the friction factor, with the exception of the onset of transition region. The decrease in the tube diameter from 2,083 to 1,600 to 1,372 μm showed the onset of transition region shifted from Reynolds number of 1,500 to 1,700 to 1,900, respectively.

As the tube diameter is further decreased, the friction factor profiles also shifted (see Figure 8). When the tube diameter is decreased from 1,372 to 1,067 μm, another group of similar

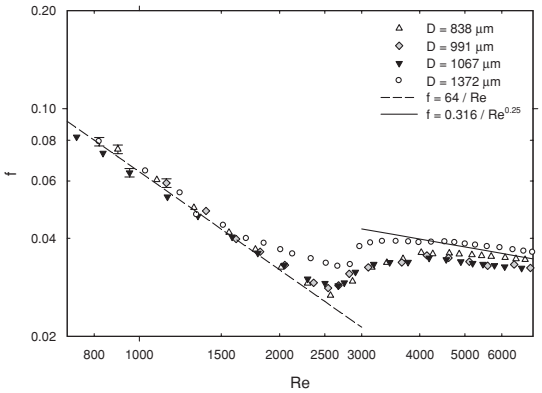

Figure 8 Transition region of stainless-steel tubes with diameters from 1,372 to 838 μm.

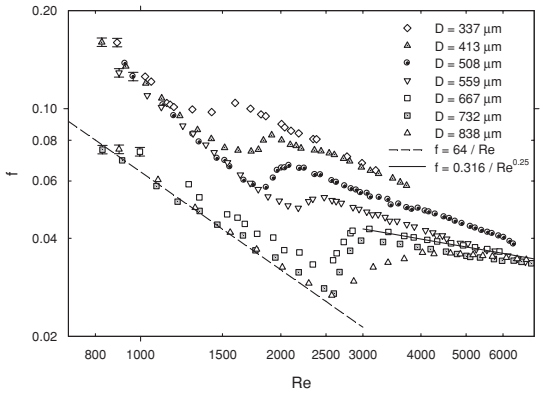

Figure 9 Transition region of stainless-steel tubes with diameters from 838 to 337 μm.

friction factor profiles in the transition region is seen. Figure 8 shows that the decrease in tube diameter from 1,067 to 838 μm did not significantly affect the profile of the friction factor. Since the 991 μm diameter tube is only 7% smaller than the 1,067 μm diameter tube, it is expected that they have the same friction factor profile and transition range ($2{,}000 < Re < 4{,}000$). However, as the diameter is decreased from 991 to 838 μm, there is a slight noticeable change in the friction factor profile, with the onset of the transition region shifted from Reynolds number of 2,000 to 2,200 and an increase in the depth of the trough in the transition region.

Figure 9 shows that further decrease in the tube diameter from 838 to 337 μm caused the transition region to become significantly narrower. The onset of transition region for 732- and 667-μm tubes is the same as that of the 838-μm tube, at Reynolds number of 2,200. However, the end of transition region is shifted forward to Reynolds number of 3,000, making the transition region of the 732 and 667 μm tubes narrower than that of the 838 μm tube. Further decrease in the tube diameter from 667 to 337 μm caused the onset and end of the transition region to shift to lower Reynolds numbers, while the transition range became narrower. The decrease in the tube diameter from 732 to 337 μm also caused the friction factor profile to shift higher. This suggests that the effect of surface roughness may be beginning to influence the friction factor. Also, the irregularities in the stainless-steel tube at such small scale, as illustrated in Figure 3, could have contributed to the shift in the friction factor profile.

The constricted flow diameter (D_{cf}), proposed by Kandlikar et al. [14], can be determined based on the inner diameter tolerances specified by the manufacturer and the results from both SPM and SEM measurements. Using the concept of constricted flow diameter, as in Eq. (1), the roughness height (ε) of the tubes can be estimated using the determined constricted flow diameter (D_{cf}). To compare the current experimental work with the work of others, friction factor data points plotted by Brackbill and Kandlikar [16] for channels with varying relative roughness (Figure 1a) were extracted and plotted with current experimental data for tube with diameter of 413 μm (Figure 10). The comparison in Figure 10 verifies the notion of roughness affecting the laminar friction factors. It should be noted that the friction factors measured by Brackbill and Kandlikar [16] were from channels with surface roughness that was created systematically to be uniform and aligned. On the other hand, the tubes used in this study were obtained commercially, and the uniformity and alignment of the surface roughness in these tubes are uncertain. Thus, some discrepancies in the results of current study with the results from Brackbill and Kandlikar [16] are to be expected. In addition, results from Li et al. [9] have reported that results from rough tubes with peak–valley roughness of 3 to 4% showed 15 to 37% higher than the f·Re value of 64 in laminar region, which is in agreement with the findings of this work.

Having known the constricted flow diameter (D_{cf}), the constricted flow friction factor (f_{cf}) and the Reynolds number (Re_{cf}) can be determined using Eqs. (2) and (3), respectively. Figure

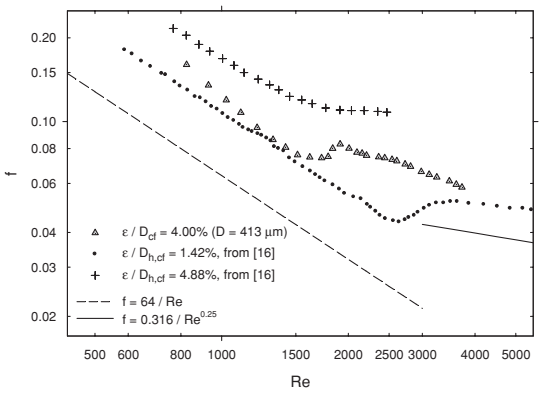

Figure 10 Comparison of friction factor data for 413 μm diameter tube with data for channels plotted by Brackbill and Kandlikar [16].

11 shows the experimental data plotted using the constricted flow friction factor (f_{cf}) and Reynolds number (Re_{cf}). When compared with the laminar friction factor theory ($f = 64/Re$), the experimental data plotted with the constricted flow parameters showed better agreement than the data plotted in Figure 9. This is another confirmation of the observation by Brackbill and Kandlikar [16] that roughness has effects on the friction factor in the laminar region (Figure 1b). To improve the agreement with laminar friction factor theory, the experimental data needs to be plotted with the constricted flow parameters, which in essence discounts the roughness element height and only considers the free flow area corresponding to the constricted flow diameter (D_{cf}).

To verify that roughness affects the onset of transition from laminar flow, the correlation (Eq. (4)) proposed by Brackbill and Kandlikar [16] was applied to the critical Reynolds numbers summarized in Table 1. The comparison of Eq. (4) with the critical Reynolds numbers observed in current experimental work is shown in Figure 12. The correlation shows favorable comparison with the observations of this experimental study. The majority of the data points compared were within the ±13% average error band reported in [16], while most of the data points compared were within ±20% error band. Thus, the experimental

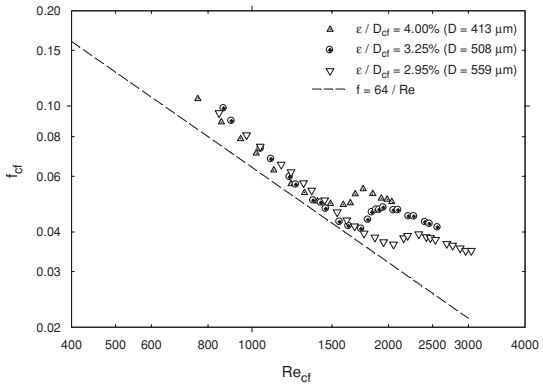

Figure 11 Experimental data from selected tubes plotted with the constricted flow parameters f_{cf} and Re_{cf} for comparison with laminar region friction factor theory.

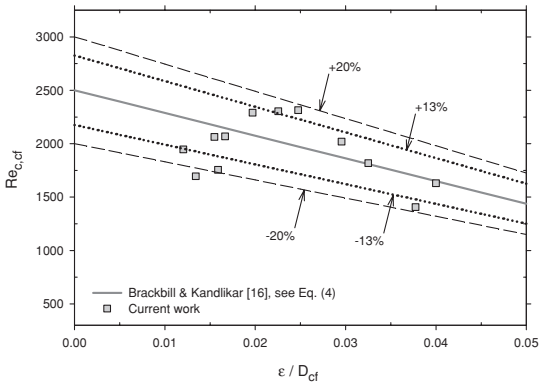

Figure 12 Comparison of critical Reynolds numbers observed in current work with Eq. (4) proposed by Brackbill and Kandlikar [16].

data from the current work agrees with the finding of Brackbill and Kandlikar [16] that increase in the relative roughness lowers the Reynolds numbers for the onset of the transition region. It should be noted that the correlation (Eq. (4)) proposed by Brackbill and Kandlikar [16] was recommended for channels. The use of the correlation here with data from tubes is to merely demonstrate that increase in the relative roughness causes early transition, which was seen in both small sized tubes and channels. Further validation with data from both tubes and channels is necessary to confirm the performance and feasibility of Eq. (4) for both tubes and channels.

CONCLUSIONS

This study systematically investigated the experimental results for the single-phase flow characteristics of distilled water in stainless-steel mini- and microtubes of diameters ranging from 2,083 to 337 μm. The sensitivity of the instruments and careful, systematic experimental methodology are the key to obtaining the accurate measurements necessary for this type of research. Improper use of pressure-sensing diaphragms could easily lead to erroneous conclusions about the flow phenomena in mini- and microtubes in addition to improper representation of the transition region. With so much left to explore in terms of the effects of surface roughness and diameter on mini- and microtube flow, neither of these outcomes can be deemed tolerable.

Decrease in tube diameters and increase in relative roughness have been found to influence friction factor, even in the laminar region. These findings were confirmed with results from [9, 14–16]. In addition to friction factor, decrease in tube diameters and increase in relative roughness have shown that the onset of transition from laminar flow occurred at lower Reynolds numbers. Also, the experimental results indicated that the Reynolds number range for transition flow becomes narrower with the decrease in the tube diameter.

When measuring the friction factor and determining the onset of transition flow for mini- and microtubes, both the diameter and the roughness height have to be accounted for. As shown in this work, relative roughness affects the friction factor and the critical Reynolds number, and both the diameter and the roughness height affect the relative roughness. When the tube diameter is accounted for while the surface roughness is ignored, the discrepancy of the friction factor with classical theory cannot be properly explained.

NOMENCLATURE

D	tube inner diameter, m
D_{cf}	constricted flow diameter, m
$D_{h,cf}$	constricted flow hydraulic diameter, m
f	Darcy friction factor
f_{cf}	Darcy friction factor based on constricted diameter
f_F	Fanning friction factor (= f/4)
f_{Fcf}	Fanning friction factor based on constricted diameter (= f_{cf}/4)
L	tube length, m
$\dot{m}$	mass flow rate, kg/s
R_a	average roughness from SPM, m
R_{max}	maximum roughness profile peak height from SPM, m
R_q	root mean square roughness from SPM, m
Re	Reynolds number
Re_{cf}	Reynolds number based on constricted diameter
$Re_{c,cf}$	critical Reynolds number based on constricted diameter
$Re_{c,o}$	critical Reynolds number for ($\varepsilon/D_{h,cf} = 0$)
RR	relative roughness
SEM	scanning electron microscope
SPM	scanning probe microscope
V	average velocity, m/s

Greek Symbols

Δp	pressure drop, Pa
ε	roughness height, m
μ	absolute viscosity, Pa·s
ρ	density, kg/m^3

REFERENCES

[1] Choi, S. B., Barron, R. F., and Warrington, R. O., Fluid Flow and Heat Transfer in Microtubes, *Proceedings of Winter Annual Meeting of the ASME Dynamic Systems and Control Division*, Atlanta, GA, vol. 32, pp. 123–134, 1991.

[2] Yu, D., Warrington, R., Barron, R., and Ameel, T., Experimental and Theoretical Investigation of Fluid Flow and Heat Transfer in Microtubes, *Proceedings of the 1995 ASME/JSME Thermal Engineering Joint Conference*, Maui, HI, vol. 1, pp. 523–530, 1995.

[3] Hwang, Y. W., and Kim, M. S., The Pressure Drop in Microtubes and the Correlation Development, *International Journal of Heat and Mass Transfer*, vol. 49, no. 11–12, pp. 1804–1812, 2006.

[4] Yang, C. Y., and Lin, T. Y., Heat Transfer Characteristics of Water Flow in Micro Tubes, *Experimental Thermal and Fluid Science*, vol. 32, no. 2, pp. 432–439, 2007.

[5] Rands, C., Webb, B. W., and Maynes, D., Characterization of Transition to Turbulence in Microchannels, *International Journal of Heat and Mass Transfer*, vol. 49, no. 17–18, pp. 2924–2930, 2006.

[6] Mala, Gh. M., and Li, D., Flow Characteristics of Water in Microtubes, *International Journal of Heat and Fluid Flow*, vol. 20, no. 2, pp. 142–148, 1999.

[7] Celata, G. P., Cumo, M., Guglielmi, M., and Zummo, G., Experimental Investigation of Hydraulic and Single-Phase Heat Transfer in 0.130-mm Capillary Tube, *Nanoscale and Microscale Thermophysical Engineering*, vol. 6, no. 2, pp. 85–97, 2002.

[8] Kandlikar, S. G., Joshi, S., and Tian, S., Effect of Surface Roughness on Heat Transfer and Fluid Flow Characteristics at Low Reynolds Numbers in Small Diameter Tubes, *Heat Transfer Engineering*, vol. 24, no. 3, pp. 4–16, 2003.

[9] Li, Z. X., Du, D. X., and Guo, Z. Y., Experimental Study on Flow Characteristics of Liquid in Circular Microtubes, *Nanoscale and Microscale Thermophysical Engineering*, vol. 7, no. 3, pp. 253–265, 2003.

[10] Zhao, Y., and Liu, Z., Experimental Studies on Flow Visualization and Heat Transfer Characteristics in Microtubes, *Proceedings of the 13th International Heat Transfer Conference*, Sydney, Australia, MIC-12, 2006.

[11] Tang, G. H., Li, Z., He, Y. L., and Tao, W. Q., Experimental Study of Compressibility, Roughness and Rarefaction Influences on Microchannel Flow, *International Journal of Heat and Mass Transfer*, vol. 50, no. 11–12, pp. 2282–2295, 2007.

[12] Kandlikar, S. G., Roughness Effects at Microscale—Reassessing Nikuradse's Experiments on Liquid Flow in Rough *Tubes, Bulletin of the Polish Academy of Sciences*, vol. 53, no. 4, pp. 343–349, 2005.

[13] Nikuradse, J., Laws of Flow in Rough Pipes (English Translation), *NACA Technical Memorandum* 1292, 1950.

[14] Kandlikar, S. G., Schmitt, D., Carrano, A. L., and Taylor, J. B., Characterization of Surface Roughness Effects on Pressure Drop in Single-Phase Flow in Minichannels, *Physics of Fluids*, vol. 17, 100606, 2005.

[15] Taylor, J. B., Carrano, A. L., and Kandlikar, S. G., Characterization of the Effect of Surface Roughness and Texture on Fluid Flow—Past, Present, and Future, *International Journal of Thermal Sciences*, vol. 45, pp. 962–968, 2006.

[16] Brackbill, T. P., and Kandlikar, S. G., Effect of Low Uniform, Relative Roughness on Single-Phase Friction Factors in Microchannels and Minichannels, *Proceedings of the 5th International Conference on Nanochannels, Microchannels and Minichannels*, Puebla, Mexico, ICNMM2007–30031, 2007.

[17] Young, P. L., Brackbill, T. P., and Kandlikar, S. G., Estimating Roughness Parameters Resulting from Various Machining Techniques for Fluid Flow Applications, *Heat Transfer Engineering*, vol. 30, no. 1–2, pp. 78–90, 2009.

[18] Brackbill, T. P. and Kandlikar, S. G., Effect of Sawtooth Roughness on Pressure Drop and Turbulent Transition in Microchannels, *Heat Transfer Engineering*, vol. 28, no. 8–9, pp. 662–669, 2007.

[19] Celata, G. P., Lorenzini, M., Morini, G. L., and Zummo, G., Friction Factor in Micropipe Gas Flow under Laminar, Transition and Turbulent Flow Regime, *International Journal of Heat and Fluid Flow*, vol. 30, no. 5, pp. 814–822, 2009.

[20] Krishnamoorthy, C. and Ghajar, A. J., Single-Phase Friction Factor in Micro-Tubes: A Critical Review of Measurement, Instrumentation and Data Reduction Techniques from 1991–2006, *Proceedings of the 5th International Conference on Nanochannels, Microchannels and Minichannels*, Puebla, Mexico, ICNMM2007-30022, 2007.

[21] Kline, S. J., and McClintock, F. A., Describing Uncertainties in Single-Sample Experiments, *Mechanical Engineering*, vol. 75, no. 1, pp. 3–8, 1953.

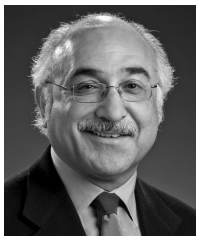

Afshin J. Ghajar is a Regents Professor and Director of Graduate Studies in the School of Mechanical and Aerospace Engineering at Oklahoma State University Stillwater, Oklahoma, and a Honorary Professor of Xi'an Jiaotong University, Xi'an, China. He received his B.S., M.S., and Ph.D., all in mechanical engineering, from Oklahoma State University. His expertise is in experimental and computational heat transfer and fluid mechanics. Dr. Ghajar has been a summer research fellow at Wright Patterson AFB (Dayton, Ohio) and Dow Chemical Company (Freeport, Texas). He and his coworkers have published over 150 reviewed research papers. He has received several outstanding teaching/service awards, such as the Regents Distinguished Teaching Award; Halliburton Excellent Teaching Award; Mechanical Engineering Outstanding Faculty Award for Excellence in Teaching and Research; Golden Torch Faculty Award for Outstanding Scholarship, Leadership, and Service by the Oklahoma State University/National Mortar Board Honor Society; and recently the College of Engineering Outstanding Advisor Award. Dr. Ghajar is a Fellow of the American Society of Mechanical Engineers (ASME), *Heat Transfer Series* editor for Taylor & Francis/CRC Press, and editor-in-chief of *Heat Transfer Engineering*. He is also the co-author of the fourth edition of Cengel and Ghajar, *Heat and Mass Transfer – Fundamentals and Applications*, McGraw-Hill, 2010.

Clement C. Tang is a Ph.D. candidate in the School of Mechanical and Aerospace Engineering at Oklahoma State University, Stillwater, Oklahoma. He received his B.S. and M.S. degrees in mechanical engineering from Oklahoma State University. His areas of specialty are single-phase flow in mini- and microtubes and two-phase flow heat transfer.

Wendell L. Cook is a graduate student in the School of Mechanical and Aerospace Engineering at Oklahoma State University, Stillwater, Oklahoma. He received his B.S. and M.S. degrees in mechanical engineering from Oklahoma State University. He recently started his Ph.D. studies in mechanical engineering focusing on single-phase and two-phase flow in mini- and microchannels.